

# Electrical manipulation of magnetic domain structure in van der Waals ferromagnetic $\text{Fe}_3\text{GaTe}_2$ using ferroelectric PMN-PT single crystal

Riku Iimori,<sup>1</sup> Yuta Kodani,<sup>1</sup> Shaojie Hu,<sup>1,2</sup> and Takashi Kimura<sup>1,3,\*</sup>

<sup>1</sup>*Department of Physics, Kyushu University,*

*744 Motooka, Fukuoka, 819-0395, Japan*

<sup>2</sup>*College of Integrated Circuits and Optoelectronic Chips,*

*Shenzhen Technology University, 3002 Lantian Road,*

*Pingshan District, Shenzhen Guangdong, China, 518118*

<sup>3</sup>*Recerch Center for Semiconductor and Device Ecosystem,*

*Kyushu University, 6-1 Kasugakoen, Kasuga, 816-8580, Japan.*

(Dated: June 12, 2025)

## Abstract

Two-dimensional (2D) van der Waals (vdW) ferromagnets have emerged as promising materials for spintronic applications due to their unique magnetic properties and tunability. Controlling ferromagnetism via external stimuli is critical for both fundamental research and device integration. In particular, modulation of magnetic anisotropy and exchange interactions through strain offers a viable pathway for functional control. Owing to their weak interlayer coupling, vdW ferromagnets exhibit pronounced sensitivity to strain, enabling effective tuning of their magnetic states. In this study, we investigate electric-field-induced magnetoelectric coupling in the above-room-temperature vdW ferromagnet  $\text{Fe}_3\text{GaTe}_2$  integrated on a ferroelectric PMN-PT substrate. We demonstrate that application of an electric field leads to a substantial reduction in coercive force along with dynamic reconfiguration of the magnetic domain structure. These effects are attributed to electric-field-induced modulation of the vdW interlayer gap and enhancement of the DzyaloshinskiiMoriya interaction. Our findings reveal a strong interplay between electric fields and magnetism in vdW systems, offering a viable route toward the development of low-power, multifunctional magnetic devices. This work establishes a foundation for the electric-field control of magnetic properties in vdW ferromagnets and highlights their potential in next-generation spintronic technologies.

---

\* Corresponding author: t-kimu@phys.kyushu-u.ac.jp

## I. INTRODUCTION

Two-dimensional (2D) van der Waals (vdW) ferromagnets have garnered significant attention due to their potential to host novel magnetic phenomena and their applicability in low-dimensional spintronic systems [1–8]. The distinctive crystal structure of these materials, composed of atomic layers with chemically inert surfaces held together by weak vdW interactions, provides an unparalleled platform for exploring the interplay between 2D material properties and magnetism [1, 9–13]. This structural configuration enables the coexistence of low dimensionality and magnetic order, leading to intriguing phenomena such as flat-band magnetism [14, 15], the tunable quantum anomalous Hall effect [16–20], and room-temperature magnetic skyrmions [21–25]. From a technological perspective, vdW ferromagnets are particularly attractive because of their compatibility with the fabrication of atomic-layer devices via mechanical exfoliation. Their ultra-thin and mechanically robust nature makes them ideal candidates for flexible and stretchable electronic components, including wearable devices [26, 27]. These properties also position vdW ferromagnets as promising materials for micro-electro-mechanical systems (MEMS) sensors, enabling novel operational mechanisms.

Despite these advantages, the stability of ferromagnetic order in 2D vdW materials remains a significant challenge. Although some materials exhibit Curie temperatures ( $T_C$ ) near room temperature [28, 29], the inherently low magnetic moments and susceptibility to thermal fluctuations in 2D systems hinder their practical applicability. As predicted by the Mermin-Wagner theorem, isotropic 2D systems with short-range interactions cannot sustain long-range magnetic order [30]. However, magnetic anisotropy can stabilize such order, making it a critical parameter in defining the ferromagnetic properties of 2D materials. Addressing these challenges requires the discovery and development of vdW materials with enhanced magnetic anisotropy and stronger ferromagnetic interactions. One promising candidate is  $\text{Fe}_3\text{GaTe}_2$ , a vdW ferromagnet that exhibits ferromagnetic order above room temperature ( $T_C \sim 365$  K) with pronounced perpendicular magnetic anisotropy [31]. Additionally,  $\text{Fe}_3\text{GaTe}_2$  demonstrates high electrical and thermal spin-conversion efficiencies [32], positioning it as a key material for next-generation spintronic devices. Building on these findings, we investigated the impact of applied pressure on the magnetic properties of  $\text{Fe}_3\text{GaTe}_2$  thin films [33]. Our study revealed that pressure systematically reduces the vdW interlayer gap, thereby enhancing perpendicular magnetic anisotropy at room temperature under relatively low pressures (below 1 GPa). Such behavior is rarely observed in conventional three-

dimensional magnetic materials. These results underscore a strong coupling between the vdW gap and magnetic anisotropy, highlighting the exceptional pressure responsiveness of  $\text{Fe}_3\text{GaTe}_2$ . This discovery provides critical insights into the tunability of magnetic properties in 2D vdW ferromagnets, paving the way for innovative applications in spintronics and flexible electronics.

Expanding upon the idea of pressure-modulated magnetism in  $\text{Fe}_3\text{GaTe}_2$ , we explored the potential for significant modulation of magnetic properties induced by in-plane strain transmitted from a substrate. Specifically, we investigated the use of ferroelectric substrates, where strain can be dynamically controlled through the application of an electric field. Previous studies have extensively analyzed field-induced modulation of magnetic properties in magnetic-ferroelectric hybrid devices [34–39]. The ferroelectric piezoelectric effect enables strain-mediated magnetic modulation solely via electric fields, eliminating current losses and offering a promising approach for nonvolatile memory technologies based on novel operating principles. Moreover, the anisotropic piezoelectric strain and strain gradients generated by ferroelectric substrates can introduce additional symmetry breaking in vdW ferromagnets, potentially giving rise to emergent magnetic phenomena. To leverage these effects, we combined the ferroelectric piezoelectric properties of the substrate with the pronounced magnetoelastic coupling observed in  $\text{Fe}_3\text{GaTe}_2$ , targeting effective electric-field modulation of its magnetic behavior.

In this study, we employed the ferroelectric crystal  $0.7\text{Pb}(\text{Mg}_{1/3}\text{Nb}_{2/3})\text{O}_3\text{-}0.3\text{PbTiO}_3$  (PMN-PT), selected for its excellent ferroelectric characteristics, including a Curie temperature ( $T_C$ ) of approximately 416 K, a high piezoelectric charge coefficient ( $d_{33} \sim 2000$  pC/N), and an electromechanical coupling factor ( $k_{33} \sim 0.94$ ) [40, 41]. As illustrated in Fig. 1(a), we integrated PMN-PT with  $\text{Fe}_3\text{GaTe}_2$  to examine electric-field-induced effects on the magnetic properties of the vdW ferromagnet. Our experimental results demonstrate that the magnetic domain structure in  $\text{Fe}_3\text{GaTe}_2$  can be effectively manipulated at room temperature through the inverse piezoelectric effect of PMN-PT under an applied electric field. These findings provide critical insights into the magnetic behaviors at vdW ferromagnet/ferroelectric interfaces and underscore the potential for energy-efficient electric-field control of magnetic structures. This work highlights a pathway for developing advanced spintronic devices with reduced power consumption and enhanced functional tunability.

## II. RESULTS AND DISCUSSION

To investigate the magnetic properties of the  $\text{Fe}_3\text{GaTe}_2/\text{PMN-PT}$  heterostructure, we performed anomalous Hall effect (AHE) measurements. Figure 3(c) shows the transverse resistance ( $R_{xy}$ ) curves observed at various temperatures. For ferromagnetic materials, the Hall resistance can be expressed as [42–44]:

$$R_{xy} = R_{\text{OHE}}B_z + R_{\text{AHE}}M_z, \quad (1)$$

where the first term represents the ordinary Hall effect (OHE), and the second term corresponds to the anomalous Hall effect (AHE). The OHE contribution was neglected in this study due to its negligible magnitude compared to the dominant AHE component. The  $R_{xy}$  curve at room temperature ( $T = 297$  K) exhibits a nearly perfect rectangular hysteresis loop, indicative of robust perpendicular magnetic anisotropy under the standard conditions. Notably, the  $\text{Fe}_3\text{GaTe}_2$  film prepared on a PMN-PT substrate displayed a more pronounced fully magnetized state at zero magnetic field compared to a similar film deposited on a thermally oxidized silicon substrate ( $\text{SiO}_2/\text{Si}$ ). As the temperature increased beyond room temperature, the AHE curves revealed that the magnetization reversal process was accompanied by the formation of multi magnetic domains prior to achieving full saturation. Figure 3(d) illustrates the temperature dependence of the AHE resistance ( $\Delta R_{\text{AHE}}$ ). Here,  $2\Delta R_{\text{AHE}}$  is defined as the difference in transverse resistance between magnetic fields  $\mu_0H = +185$  mT and  $\mu_0H = -185$  mT. Here, we performed a fitting of  $R_{xy}$  vs.  $T$  based on the relationship  $R_{xy} \propto (1 - T/T_C)^\beta$ . As a result, the Curie temperature  $T_C$  of the ferromagnetic phase was determined to be  $\sim 340$  K, which is consistent with the values reported in previous studies [31–33].

We further examined the effect of an applied electric field on the AHE behavior of the  $\text{Fe}_3\text{GaTe}_2/\text{PMN-PT}$  heterostructure. Figures 4(a) and 4(b) present the AHE curves for electric fields ranging from  $-12$  kV/cm to  $+12$  kV/cm. The results reveal that the rectangular hysteresis loop evolves into a magnetic hysteresis loop characterized by a multi-domain structure under the application of an electric field ( $E_{[001]}$ ). This transformation was dependent on the magnitude of  $E_{[001]}$  but showed minimal sensitivity to the polarity of the spontaneous electric dipole in the PMN-PT.

To further elucidate the magnetization process, we evaluated the domain nucleation field ( $H_n$ ) and the saturation field ( $H_s$ ), as shown in Figs. 5(a) and 5(b). As previously described, the application of an electric field transitions the magnetization process from an almost coherent rotation to a

reversal mechanism associated with the formation of multi-domains. Figures 5(a) and 5(b) present the dependence of  $H_n$  and  $H_s$  on the electric field ( $E_{[001]}$ ), where  $E_{[001]}$  was initially swept from +12 kV/cm to -12 kV/cm and then returned to +12 kV/cm.  $H_n$  decreases monotonically with increasing electric field, exhibiting a reduction of approximately 70 % under an applied field of 12 kV/cm. Notably,  $H_n$  displays a marked decrease with increasing magnitude of  $E_{[001]}$ , forming a butterfly-shaped profile consistent with strain curves observed in piezoelectric materials. This behavior suggests that the electric-field effect on  $H_n$  in  $\text{Fe}_3\text{GaTe}_2$  originates from strain induced by the inverse piezoelectric effect of the PMN-PT substrate. Referring to the strain curve of the PMN-PT substrate in Fig. 2(d), compressive in-plane strain is generated upon the application of  $E_{[001]}$ . This strain is transferred to the  $\text{Fe}_3\text{GaTe}_2$  layer, causing expansion along the *c*-axis via the Poisson effect, particularly within the van der Waals (vdW) gap. Conversely, a slight increase in  $H_s$  was observed near zero electric field; however, this variation remained within the error margins. We also observed that the Curie temperature ( $T_C$ ) of  $\text{Fe}_3\text{GaTe}_2$  is insensitive to electric fields ( $E_{[001]}$ ) up to 6 kV/cm, as presented in Fig. 3(e). To avoid potential damage to the PMN-PT substrate at elevated temperatures, the field dependence of  $T_C$  was not evaluated beyond 6 kV/cm. The absence of significant field dependence of  $T_C$  aligns with the minimal field sensitivity of  $H_s$ .

To further investigate the origin of electric-field effects on the magnetic properties of the  $\text{Fe}_3\text{GaTe}_2$ /PMN-PT heterostructure, we analyzed the difference  $\Delta H$  between the saturation field  $H_s$  and the nucleation field  $H_n$  of the multi-domain structure. This difference characterizes the stabilization region of metastable domains. Figure 5(c) illustrates the stabilization field range of multi-domains as a function of the electric field. The results reveal that higher electric fields enhance the stability of the multi-domain structure, indicating the pivotal role of electric-field-induced strain in modulating the magnetic properties of vdW ferromagnetic systems.

To understand the electric-field dependence of  $\Delta H$ , we simply propose that the observed reduction in perpendicular magnetic anisotropy arises from an expansion of the van der Waals (vdW) gap. Our previous studies on the pressure effects in  $\text{Fe}_3\text{GaTe}_2$  have demonstrated that applying the pressure significantly enhances perpendicular magnetic anisotropy [33]. According to the analysis, the pressure is known to induce the modification of the vdW gap as well as the lattice parameters effectively, namely a few percent per GPa. On the other hand, as shown in Fig. 2(d), the induced strain via the inverse piezo electric effect is one order smaller than that by the pressure application (see also Supplementary Note 4). This means that the observed enhancement  $\Delta H$  due to the electric field cannot be explained only by the modification of the PMA due to the reduction in the

vdW gap.

To further discuss the mechanisms underlying the observed effects more quantitatively, we take into account the Dzyaloshinskii-Moriya interaction (DMI). The magnetic energy density  $w_e$  for the present system can be expressed as:

$$w_e = -A(\nabla \mathbf{m})^2 - K_{\text{ani}} m_z^2 + D \mathbf{m} \cdot (\nabla \times \mathbf{m}), \quad (2)$$

where  $A$  represents the exchange stiffness constant,  $K_{\text{ani}}$  is the magnetic anisotropy constant, and  $D$  denotes the DMI constant. With regard to the ferromagnetic exchange interaction in  $\text{Fe}_3\text{GaTe}_2$ , our observations reveal that the Curie temperature  $T_C$  remains unchanged up to  $E_{[001]} = 6 \text{ kV/cm}$  as indicated in Fig. 3(e). Additionally, as shown in Fig. 5(a), the saturation field ( $H_s$ ) displays minimal sensitivity to the applied electric field. Furthermore, the in-plane strain in the PMN-PT substrate induced by the electric field is less than 0.03%. These results strongly support the hypothesis that the ferromagnetic exchange stiffness constant ( $A$ ) within the 2D layers of  $\text{Fe}_3\text{GaTe}_2$  is not significantly influenced by the application of the electric field.

Although the strain induced by the electric field is relatively small, it permeates the entire thickness of the  $\text{Fe}_3\text{GaTe}_2$  layer. The vdW gap is notably sensitive to strain, which modulates the perpendicular magnetic anisotropy. However, as previously discussed, these strain-induced effects alone cannot fully account for the significant reduction in the nucleation field  $H_n$  under the electric field application. Importantly, the strain decreases progressively with distance from the interface, creating a strain gradient that suggests the relevance of the DMI. An enhancement in DMI can lead to the formation of non-collinear spin structures, such as skyrmions, in ferromagnetic materials. Notably, room-temperature skyrmions attributed to DMI have been reported in  $\text{Fe}_3\text{GaTe}_2$  [22–25]. DMI arises from the interplay of spatial inversion symmetry breaking and strong spin-orbit coupling. In the  $\text{Fe}_3\text{GaTe}_2/\text{PMN-PT}$  heterostructure studied here, strain gradients due to strain relaxation significantly break symmetry along the out-of-plane direction. Additionally, the anisotropic strain introduced by the single-crystal PMN-PT substrate, characterized by its four-fold symmetry, disrupts the intrinsic hexagonal symmetry of  $\text{Fe}_3\text{GaTe}_2$ . These combined factors contribute to the enhancement of DMI in  $\text{Fe}_3\text{GaTe}_2$ , as illustrated in Fig. 5(e).

To further investigate these phenomena, direct observations of magnetic domain behavior under electric field modulation would provide valuable insights. The ability to fabricate few-atomic-layer  $\text{Fe}_3\text{GaTe}_2$  films directly on PMN-PT with clean interfaces would allow for maximized strain coupling and could unveil more pronounced or novel electric-field effects intrinsic to the ultrathin

regime. The interface multiferroic structure formed by  $\text{Fe}_3\text{GaTe}_2$  on PMN-PT demonstrates the potential for controlling magnetic domain states with minimal electric power consumption. This capability offers promising applications in electric-field-driven micro-electromechanical systems (MEMS) and next-generation memory devices.

### III. CONCLUSIONS

We experimentally investigated the electric-field effects on the magnetic properties of a heterostructure composed of the vdW ferromagnet  $\text{Fe}_3\text{GaTe}_2$  and the ferroelectric PMN-PT. To evaluate the magnetic properties, AHE measurements were performed under varying back-gate electric fields and temperatures. Application of an electric field resulted in a significant reduction of the domain nucleation field and markedly altered the magnetization reversal mechanism from coherent rotation in a single-domain state to the formation of a multi-domain structure. In contrast, no notable change in the Curie temperature, associated with ferromagnetic exchange interactions, was observed under electric field application. Our analysis revealed that the inverse piezoelectric effect induced by the PMN-PT expanded the vdW gap, which not only weakened the interlayer perpendicular magnetic anisotropy but also enhanced the DMI in  $\text{Fe}_3\text{GaTe}_2$  through symmetry reduction. These findings highlight the strong magneto-elastic coupling properties of vdW ferromagnets and demonstrate the potential for electric-field-driven control of magnetic structures with minimal power consumption. This approach paves the way for advanced applications in next-generation spintronic devices.

---

- [1] Gong, Cheng, *et al.* Discovery of intrinsic ferromagnetism in two-dimensional van der Waals crystals. *Nature* **546**, 265-269 (2017).
- [2] Zhong, Ding, *et al.* Van der Waals engineering of ferromagnetic semiconductor heterostructures for spin and valleytronics. *Science advances* 3(5), e1603113 (2017).
- [3] Zhang, Wen, *et al.* Van der Waals magnets: wonder building blocks for two-dimensional spintronics?. *InfoMat* 1(4), 479-495 (2019).
- [4] Li, Hui, Shuangchen Ruan, and Yu-Jia Zeng. Intrinsic van der Waals magnetic materials from bulk to the 2D limit: new frontiers of spintronics. *Advanced Materials* 31(27), 1900065 (2019).
- [5] Sierra, J.F., Fabian, J., Kawakami, R.K. *et al.* Van der Waals heterostructures for spintronics and opto-spintronics. *Nat. Nanotechnol.* **16**, 856-868 (2021).
- [6] Jiang, Xue, *et al.* Recent progress on 2D magnets: Fundamental mechanism, structural design and modification. *Applied Physics Reviews* 8(3) (2021).
- [7] Yang, Shengxue, Tianle Zhang, and Chengbao Jiang. Van der Waals magnets: Material family, detection and modulation of magnetism, and perspective in spintronics. *Advanced Science* 8(2), 2002488 (2021).
- [8] Yang, Shengxue, Tianle Zhang, and Chengbao Jiang. Van der Waals magnets: Material family, detection and modulation of magnetism, and perspective in spintronics. *Advanced Science* 8(2), 2002488 (2021).
- [9] Huang, Bevin, *et al.* Layer-dependent ferromagnetism in a van der Waals crystal down to the monolayer limit. *Nature* **546**, 270-273 (2017).
- [10] Shabbir, Babar, *et al.* Long range intrinsic ferromagnetism in two dimensional materials and dissipationless future technologies. *Applied Physics Reviews* **5**, 041105 (2018).
- [11] Fei, Zaiyao, *et al.* Two-dimensional itinerant ferromagnetism in atomically thin  $\text{Fe}_3\text{GeTe}_2$ . *Nature materials* **17**, 778-782 (2018).
- [12] Yu, Wei, *et al.* Chemically exfoliated VSe<sub>2</sub> monolayers with room-temperature ferromagnetism. *Advanced Materials* 31(40), 1903779 (2019).
- [13] Amilcar Bedoya-Pinto *et al.* Intrinsic 2D-XY ferromagnetism in a van der Waals monolayer. *Science* **374**, 616-620(2021).

- [14] KATO, Yoshihiro D., *et al.* Optical anomalous Hall effect enhanced by flat bands in ferromagnetic van der Waals semimetal. *npj Quantum Materials* **7**, 73 (2022).
- [15] G. Bouzerar. Flat band induced room-temperature ferromagnetism in two-dimensional systems. *Phys. Rev. B* **107**, 184441 (2023).
- [16] Zhang, Jiayong, *et al.* Robust quantum anomalous Hall effect in graphene-based van der Waals heterostructures. *Physical Review B* **92**, 165418 (2015).
- [17] Zou, Runling, *et al.* Intrinsic quantum anomalous Hall phase induced by proximity in the van der Waals heterostructure germanene/ $\text{Cr}_2\text{Ge}_2\text{Te}_6$ . *Physical Review B* **101**, 161108 (2020).
- [18] Li, Tingxin, *et al.* Quantum anomalous Hall effect from intertwined moiré bands. *Nature* **600**, 7890 (2021).
- [19] Bora, Mayuri, *et al.* Magnetic proximity induced valley-contrasting quantum anomalous Hall effect in a graphene- $\text{CrBr}_3$  van der Waals heterostructure. *Physical Review B* **105**, 235422 (2022).
- [20] Park, Heonjoon, *et al.* Observation of fractionally quantized anomalous Hall effect. *Nature* **622**, 7981 (2023).
- [21] Meisenheimer, P., Zhang, H., Raftrey, D. *et al.* Ordering of room-temperature magnetic skyrmions in a polar van der Waals magnet. *Nat Commun* **14**, 3744 (2023).
- [22] Li, Z., Zhang, H., Li, G. *et al.* Room-temperature sub-100nm Néel-type skyrmions in non-stoichiometric van der Waals ferromagnet  $\text{Fe}_3-x\text{GaTe}_2$  with ultrafast laser writability. *Nat Commun* **15**, 1017 (2024).
- [23] Xiaofei Hou, Haonan Wang, Binshuo Zhang, Chen Xu, Lu Sun, Zhengxian Li, Xia Wang, Ke Qu, Yurui Wei, Yanfeng Guo. Room-temperature skyrmions in the van der Waals ferromagnet  $\text{Fe}_3\text{GaTe}_2$ . *Appl. Phys. Lett.* **124**, 142404 (2024).
- [24] C. Liu, S. Zhang, H. Hao, H. Algaidi, Y. Ma, X.-X. Zhang. Magnetic Skyrmions above Room Temperature in a van der Waals Ferromagnet  $\text{Fe}_3\text{GaTe}_2$ . *Adv. Mater.* **36**, 2311022 (2024).
- [25] Ji, Yubin, *et al.* Direct Observation of Room-Temperature Magnetic Skyrmion Motion Driven by Ultra-Low Current Density in Van Der Waals Ferromagnets. *Adv. Mater.* **36**(21), 2312013 (2024).
- [26] Yao, Jiandong, and Guowei Yang. Flexible and high-performance all-2D photodetector for wearable devices. *Small* **14**(21), 1704524 (2018).
- [27] Lee, Meng Hao, and Wenzhuo Wu. 2D materials for wearable energy harvesting. *Advanced Materials Technologies* **7**(9), 2101623 (2022).

[28] May, Andrew F., *et al.* Ferromagnetism near room temperature in the cleavable van der Waals crystal  $\text{Fe}_5\text{GeTe}_2$ . *ACS nano* **6**(3), 13(4), 4436-4442 (2019).

[29] Seo, Junho, *et al.* Nearly room temperature ferromagnetism in a magnetic metal-rich van der Waals metal. *Science advances* **6**(3), eaay8912 (2020).

[30] N David Mermin and Herbert Wagner. Absence of ferromagnetism or antiferromagnetism in one-or two-dimensional isotropic heisenberg models. *Phys. Rev. Lett.* **17**, 1133 (1966).

[31] Zhang, G., Guo, F., Wu, H. *et al.* Above-room-temperature strong intrinsic ferromagnetism in 2D van der Waals  $\text{Fe}_3\text{GaTe}_2$  with large perpendicular magnetic anisotropy. *Nat Commun* **13**, 5067 (2022).

[32] Shuhan Liu, Shaojie Hu, Xiaomin Cui, Takashi Kimura. Efficient Thermo-Spin Conversion in van der Waals Ferromagnet FeGaTe. *Adv. Mater.* **2023**, 2309776 (2023).

[33] Riku Iimori, Shaojie Hu, Akihiro Mitsuda, and Takashi Kimura. Substantial enhancement of perpendicular magnetic anisotropy in van der Waals ferromagnetic  $\text{Fe}_3\text{GaTe}_2$  film due to pressure application. *Commun Mater* **5**, 235 (2024).

[34] Heron, J. T., *et al.* Electric-field-induced magnetization reversal in a ferromagnet-multiferroic heterostructure. *Phys. Rev. Lett.* **107**, 217202 (2011).

[35] C A F Vaz. Electric field control of magnetism in multiferroic heterostructures. *J. Phys.: Condens. Matter* **24**, 333201 (2012).

[36] Martin, L. W., and R. Ramesh. Multiferroic and magnetoelectric heterostructures. *Acta Materialia* **60**(6-7), 2449-2470 (2012).

[37] Morgan Trassin. Low energy consumption spintronics using multiferroic heterostructures. *J. Phys.: Condens. Matter* **28**, 033001 (2015).

[38] Hu, Jia-Mian, Long-Qing Chen, and Ce-Wen Nan. Multiferroic heterostructures integrating ferroelectric and magnetic materials. *Advanced materials* **28**(1), 15-39 (2016).

[39] Taniyama, T., Gohda, Y., Hamaya, K., and Kimura, T. Artificial multiferroic heterostructures—electric field effects and their perspectives. *Science and Technology of Advanced Materials* **25**(1), 2412970 (2024).

[40] Shrout, T. R., Chang, Z. P., Kim, N., and Markgraf, S. Dielectric behavior of single crystals near the  $(1-x)\text{Pb}(\text{Mg}_{1/3}\text{Nb}_{2/3})\text{O}_3-(x)\text{PbTiO}_3$  morphotropic phase boundary. *Ferroelectrics Letters Section* **12**(3), 63–69 (1990).

[41] Rajan, K. K., *et al.* Dielectric and piezoelectric properties of [001] and [011]-poled relaxor ferroelectric PZN-PT and PMN-PT single crystals. *Sensors and Actuators A: Physical* **133**(1), 110-116

(2007).

- [42] Emerson M. Pugh. Hall Effect and the Magnetic Properties of Some Ferromagnetic Materials. *Phys. Rev.* **36**, 1503 (1930).
- [43] E. M. Pugh and T. W. Lippert, Hall e.m.f. and Intensity of Magnetization *Phys. Rev.* **42**, 709 (1932).
- [44] Nagaosa, Naoto, *et al.* Anomalous hall effect. *Rev. Mod. Phys.* **82**, 1539 (2010).
- [45] RR. K. Zheng *et al.* Converse piezoelectric control of the lattice strain and resistance in Pr0.5Ca0.5MnO<sub>3</sub>/PMN-PT structures. *Phys. Rev. B* **75**, 024110 (2007).
- [46] Giannozzi, P. *et al.* QUANTUM ESPRESSO: a modular and open-source software project for quantum simulations of materials. *J. Phys. Condens. Matter* **21**, 395502 (2009).
- [47] Giannozzi, P. *et al.* Advanced capabilities for materials modelling with quantum ESPRESSO. *J. Phys. Condens. Matter* **29**, 465901 (2017).
- [48] Grimme, S. Semiempirical GGA-type density functional constructed with a long-range dispersion correction. *J. Comput. Chem.* **27**, 1787–1799 (2006).
- [49] Grimme, S., Antony, J., Ehrlich, S. and Krieg, H. A consistent and accurate ab initio parametrization of density functional dispersion correction (DFT-D) for the 94 elements H-Pu. *J. Chem. Phys.* **132**, 154104 (2010).

## METHODS

### Device fabrication and characterization

In the present study, we fabricated the  $\text{Fe}_3\text{GaTe}_2/\text{PMN-PT}$  heterostructure device by mechanically exfoliating single crystals consisting of  $\text{Fe}_3\text{GaTe}_2$ . The bulk  $\text{Fe}_3\text{GaTe}_2$  crystals were synthesized using a self-flux method. A mixture with a molar ratio of  $\text{Fe:Ga:Te} = 1:1:2$  was placed in an alumina crucible, vacuum-sealed in a quartz tube, and heat-treated in a muffle furnace. The temperature was ramped to  $1000\text{ }^\circ\text{C}$  within 1 hour, maintained for 24 hours, then lowered to  $880\text{ }^\circ\text{C}$  within 1 hour, and gradually cooled to  $780\text{ }^\circ\text{C}$  over 120 hours. The temperature was held at  $780\text{ }^\circ\text{C}$  for 24 hours before centrifugation was employed to separate the crystals from the Te flux. Supplementary Figure 2 presents the X-ray diffraction (XRD) spectra of the synthesized  $\text{Fe}_3\text{GaTe}_2$ , which predominantly exhibit  $(00h)$  peaks, indicating a high-quality crystal with *c*-axis orientation. In addition, the transmission electron microscopy (TEM) image clearly reveals the layered crystal structure as shown in Fig. 1(b). Figure 1(c) illustrates the Hall measurement device structure. The  $\text{Fe}_3\text{GaTe}_2$  film was mechanically exfoliated and transferred onto a (001)-oriented single-crystalline PMN-PT substrate in a nitrogen-filled glovebox. The thickness of the exfoliated  $\text{Fe}_3\text{GaTe}_2$  film was measured to be 49 nm using atomic force microscopy (AFM), as shown in the right panel of Fig. 3(b). Subsequently, electrodes were patterned using electron beam lithography and low-energy ion milling techniques. Figure 3(a) shows a scanning electron microscopy (SEM) image of the fabricated  $\text{Fe}_3\text{GaTe}_2/\text{PMN-PT}$  device. Copper (200 nm) electrodes were deposited via Joule heating evaporation under a base pressure of  $2.0 \times 10^{-6}\text{ Pa}$ . For back-gating control, silver paste was applied to the back side of the PMN-PT substrate to fabricate gate electrodes. To prevent property changes due to redox reactions, the fabricated devices were spin-coated with poly(methyl methacrylate) (PMMA).

### Electric field control using ferroelectric PMN-PT single crystals

The electric field control was performed using the programmable DC voltage source Advantest R6161. The electric field was symmetrically driven in a bipolar manner, alternating sequentially between  $|E_{\text{max}}|$  and  $-|E_{\text{max}}|$ , to prevent the retention of biased hysteresis. Furthermore, to prevent cracks caused by inhomogeneous strain, the uniform application of the gate electric field was verified using an optical microscope by confirming that the transparency changed uniformly with the application of the electric field. The detailed electric-field-induced strain characteristics of the PMN-PT were evaluated using the XRD as shown in Fig. 2(b). Figure 2(d) shows the gate field

$E_{[001]}$  dependence of the out-of-plane strain  $\varepsilon_{zz}$  ( $= \Delta c/c$ ) for the PMN-PT substrate. The strain curve was evaluated by the bragg-peak shift of the PMN-PT (003) reflection. We observed the ferroelectric hysteresis and the tensile strain of about 0.05% along the  $c$ -axis, which consistsents with the previous studies [45]. Considering the constant volume Poisson effect ( $2\varepsilon_{xx} + \varepsilon_{zz} = 0$ ), the  $c$ -axis tensile strain corresponds to an in-plane compressive strain  $\varepsilon_{xx}$  of about  $-0.03\%$ , suggesting that  $\text{Fe}_3\text{GaTe}_2$  undergoes in-plane compressive strain from the PMN-PT interface as shown in Figs. 1(c) and 2(d).

### **Magneto-electric transport properties mesurements**

The anomalous Hall effect (AHE) measurements were performed using an AC lock-in detection technique under temperature control from 300 K to 400 K. The applied current was 100  $\mu\text{A}$  at a frequency of 173 Hz. Here, the time constant of the lock-in amplifier is 100 ms and the sweep rate of the external magnetic field is 25 Oe/s. All measurements were conducted in vacuum to prevent degradation of the device during experiments. For high-temperature application from 300 K to 400 K, a ceramic heater (MC2525H) manufactured by Sakaguchi electric heaters Co., Ltd. was used, and temperature control was achieved using a DC-type temperature controller with a K-type thermocouple.

### **First-principles calculations**

To evaluate the effect of in-plane substrate strain on  $\text{Fe}_3\text{GaTe}_2$ , first-principles calculations based on density functional theory (DFT) were performed using the QUANTUM ESPRESSO package [46, 47]. We employed pseudopotentials within the projector-augmented-wave (PAW) framework, using the Perdew–Burke–Ernzerhof (PBE) generalized gradient approximation (GGA) for the exchange-correlation functional. The plane wave cutoff energy was set to 70 Ry, with a  $12 \times 12 \times 4$   $k$ -point mesh for self-consistent calculations in the Brillouin zone. To account for van der Waals interactions, we applied Grimme’s DFT-D3 dispersion correction [48, 49]. Based on the above, the lattice relaxation of bulk  $\text{Fe}_3\text{GaTe}_2$  was performed under various in-plane strain conditions to evaluate the change in the lattice parameter along the  $c$ -axis. The detailed results are provided in Supplementary Note 3.

## **DATA AVAILABILITY**

The data that support the findings of this study are available from the corresponding author upon request.

## **AUTHOR CONTRIBUTIONS**

R.I., H.S. and T.K. conceptualized and planned the project. T.K. supervised the project. R.I. fabricated samples. Y.K. evaluated the X-ray diffraction measurements with support from R.I. R.I. and Y.K. performed transport measurements. Analyses of the data were done by R.I., Y.K., H.S., and T.K. R.I. wrote the manuscript with support from K.Y, H.S. and T.K. All authors discussed the results and commented on the manuscript.

## **ACKNOWLEDGMENTS**

This work was supported by NEOD (Uncharted Territory Challenge 24000474), JSPS KAK-ENHI Grant Numbers 21H05021, 23KJ1701, and JST (CREST: JPMJCR18J1, SICORP: 22480474).

## **COMPETING INTERESTS**

The authors declare no competing interests.

## **ADDITIONAL INFORMATION**

Supplementary information is available for this paper at [xxx](#).

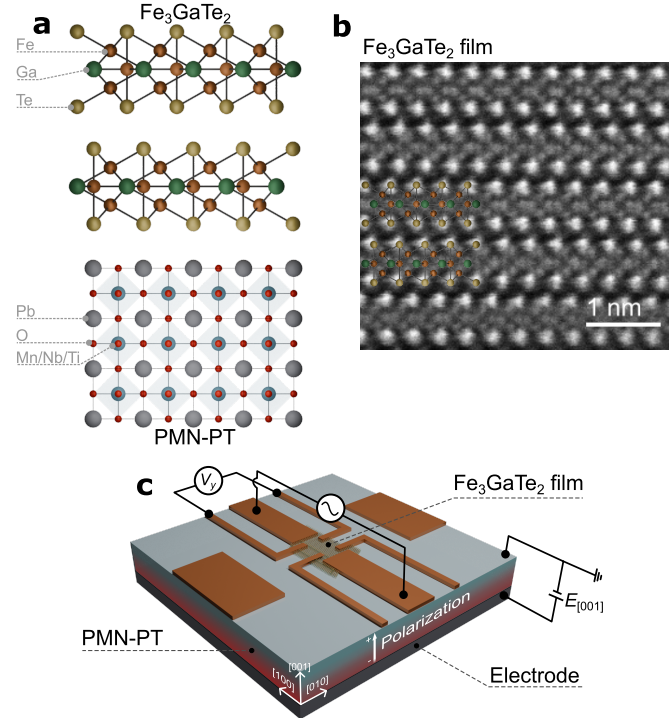


**FIG. 1. Heterostructure combining vdW ferromagnetic  $\text{Fe}_3\text{GaTe}_2$  and ferroelectric PMN-PT.** (a) Schematic of atomic structure of  $\text{Fe}_3\text{GaTe}_2$ /PMN-PT heterostructure. Here, the composition of the PMN-PT is  $0.7\text{Pb}(\text{Mg}_{1/3}\text{Nb}_{2/3})\text{O}_3\text{-}0.3\text{PbTiO}_3$ , and a  $c$ -plane cut PMN-PT substrate was used in this study. (b) Cross-sectional transmission electron microscopy (TEM) image of the  $\text{Fe}_3\text{GaTe}_2$  film. (c) Device structure for the magneto-transport measurement with circuit diagram. The electric field is applied to the ferroelectric PMN-PT substrate in a back-gate configuration. The inverse piezoelectric effect of the substrate transmits the strain to the  $\text{Fe}_3\text{GaTe}_2$ .

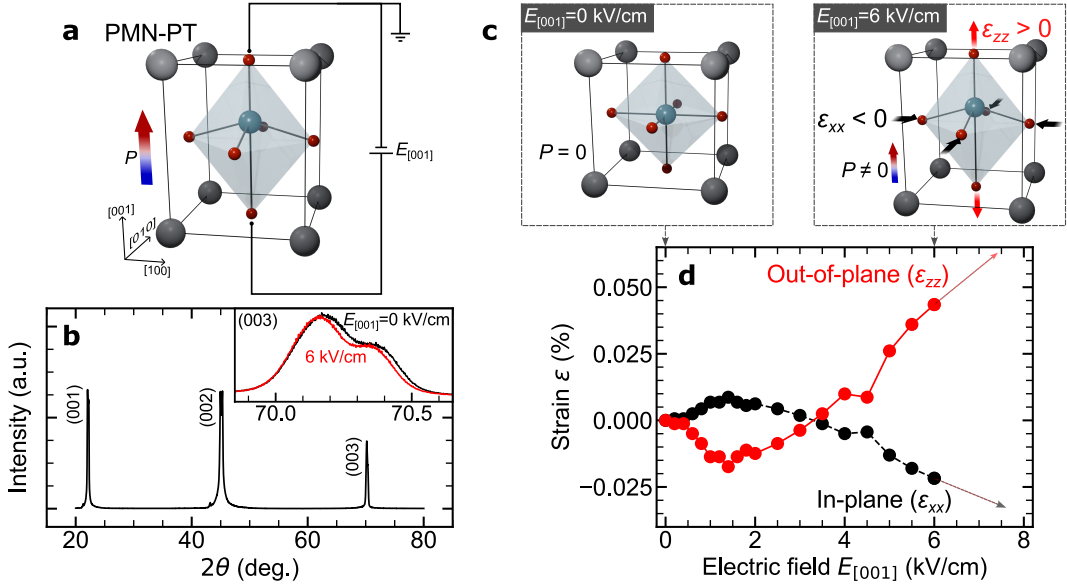
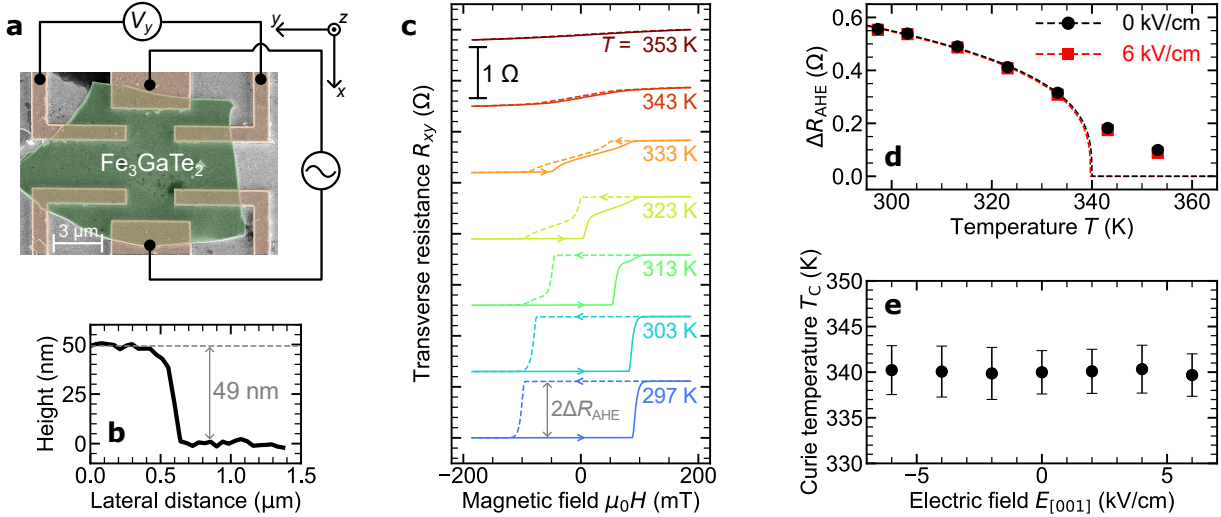
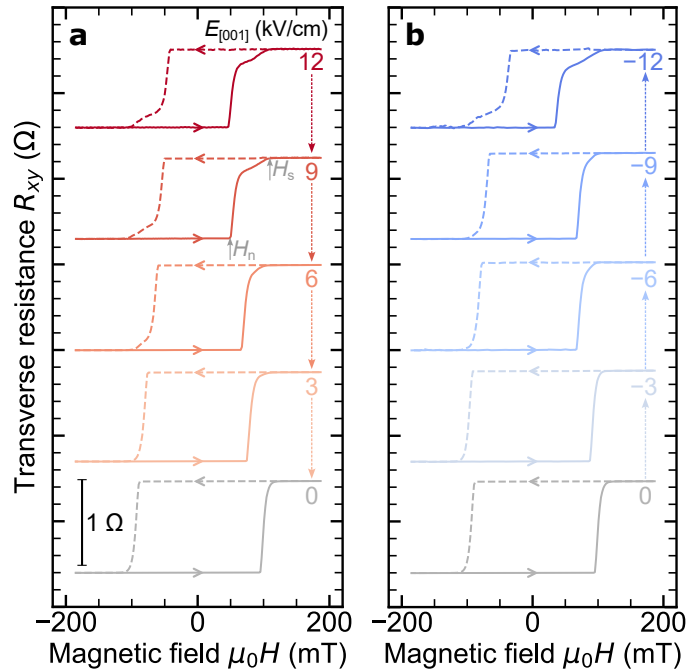


FIG. 2. **Electric field characteristics of the PMN-PT single crystal.** (a) Schematic illustration of the inverse piezoelectric effect of the PMN-PT crystal under the electric field  $E_{[001]}$ . In this study, the electric field  $E_{[001]}$  is applied along the [001] direction of PMN-PT single crystal. (b) X-ray diffraction (XRD) pattern of the PMN-PT single crystal. The inset shows the (003) spectra as a function of the back-gate electric field up to 6 kV/cm. (c) Schematic diagrams of the polarization and strain profiles under  $E_{[001]} = 0\text{ kV/cm}$  and 6 kV/cm. (d) Electric field dependence of out-of-plane strain ( $\epsilon_{zz} = \Delta c/c$ ) evaluated from the shift of the (003) XRD peak. In-plane ( $\epsilon_{xx}$ ) strain was derived based on the approximation of constant volume in the Poisson effect ( $2\epsilon_{xx} + \epsilon_{zz} = 0$ ).



**FIG. 3. Ferromagnetic properties of the  $\text{Fe}_3\text{GaTe}_2$ /PMN-PT device.** (a) Scanning electron microscope (SEM) image of the fabricated  $\text{Fe}_3\text{GaTe}_2$ /PMN-PT device together with the probe configuration. (b) Cross-sectional height profile measured by the atomic force microscopy (AFM). (c) Transverse resistance  $R_{xy}$  as a function of the applied magnetic field  $H$  along the perpendicular direction under various temperatures. (d) Temperature dependence  $T$  of the anomalous Hall resistance  $\Delta R_{\text{AHE}}$  at  $E_{[001]} = 0$  and 6 kV/cm. Curie temperature  $T_C$  of the ferromagnetism for the  $\text{Fe}_3\text{GaTe}_2$ /PMN-PT heterostructure was determined by fitting the  $R_{xy}$  vs.  $T$  data to the relationship  $R_{xy} \propto (1 - T/T_C)^\beta$ . (e) Curie temperature  $T_C$  as a function of the applied electric field  $E_{[001]}$ .



**FIG. 4. Electric-field modulated anomalous Hall resistance curves in the  $\text{Fe}_3\text{GaTe}_2/\text{PMN-PT}$  device.**  
 Room-temperature anomalous Hall resistance  $R_{xy}$  curves measured under different back-gate electric fields  $E_{[001]}$  ranging (a) from 0 to +12 kV/cm (positive direction) and (b) from 0 to -12 kV/cm (negative direction).

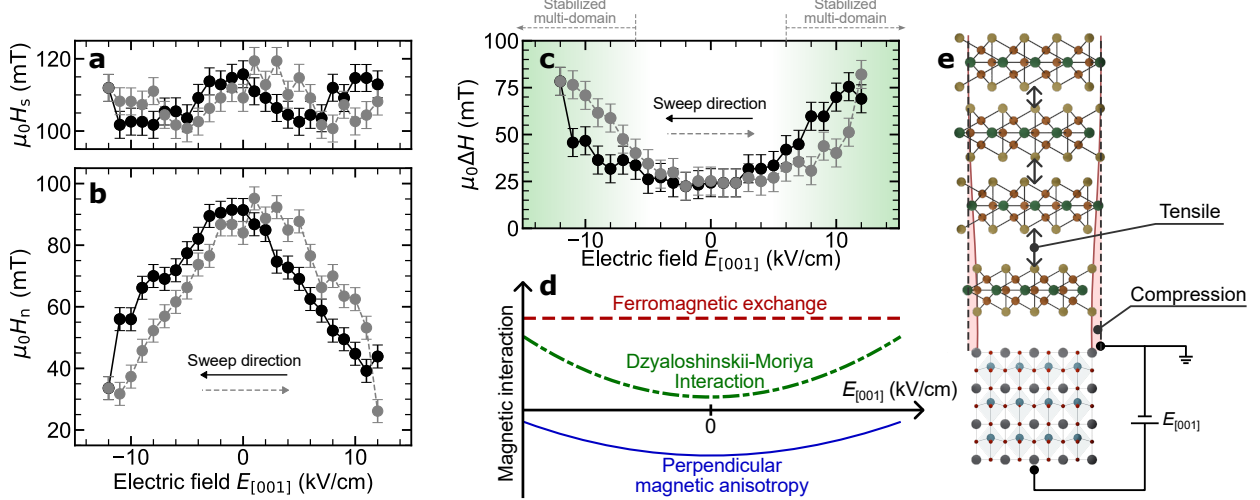


**FIG. 5. Origin of the electric field effect on the magnetic domains of the  $\text{Fe}_3\text{GaTe}_2/\text{PMN-PT}$  heterostructure.** (a) Electric field  $E_{[001]}$  dependence of the saturation magnetic field  $H_s$ . (b) the nucleation magnetic field  $H_n$  as a function of the  $E_{[001]}$ . Here, the black solid line represents the magnetic field being swept from positive to negative, while the gray dashed line indicates the opposite direction. (c) Electric field  $E_{[001]}$  dependence of the  $\Delta H$  ( $= H_s - H_n$ ) in the  $\text{Fe}_3\text{GaTe}_2/\text{PMN-PT}$  heterostructure. (d) Changes in magnetic interactions induced by electric field  $E_{[001]}$ . Since there was no significant change in the Curie temperature, the ferromagnetic interactions remained largely unaffected. On the other hand, the in-plane strain of PMN-PT expands the van der Waals gap, leading to a reduction in perpendicular magnetic anisotropy. Additionally, the change in symmetry due to the strain gradient enhances the Dzyaloshinskii-Moriya interaction. (e) Strain profile induced by the electric field in the  $\text{Fe}_3\text{GaTe}_2/\text{PMN-PT}$  structure.